Pergamon

Int. J. Heat Mass Transfer. Vol. 39, No. 3, pp. 455–465, 1996

0017-9310/96 $9.50 + 0.00

0017-9310(95)00157-3

An explicit algebraic heat-flux model for the temperature field

R. M. C. SO and T. P. SOMMER†

Mechanical and Aerospace Engineering, Arizona State University, Tempe, AZ 85287-6106, U.S.A.

(*Received* 13 *December* 1994 *and in final form* 18 *April* 1995)

Abstract—An explicit algebraic heat-flux (EAHF) model is derived by invoking the assumption of equilibrium turbulence for both the velocity and the thermal fields. Further modifications are achieved by applying an approximation technique to render the implicit heat flux vector relation explicit. Thus derived, the heat flux vector yields two terms. The first term is identical to that given by a simple thermal eddy diffusivity model, while the second term provides a correction to the streamwise heat flux. This second term is non-zero even when the streamwise mean temperature gradient is zero. It allows the modeling of the generation of a streamwise heat flux due to the interaction of the turbulent eddies with the mean temperature gradient normal to the streamwise direction. Previously derived near-wall corrections to the equations of the temperature variance and its dissipation rate are found to be equally valid for the EAHF model. The near-wall EAHF model is validated against direct numerical simulation data and experimental measurements. In addition, the calculations are also compared with those obtained from a second-order model and the simple thermal eddy diffusivity model. Two different near-wall Reynolds-stress models are used to calculate the velocity field and they are found to have little effect on the thermal field predicted by the EAHF model. In general, the results for the temperature field are in good agreement with data and are essentially unaffected by the second term in the EAHF model. On the other hand, the prediction of the streamwise heat flux is in good agreement with that given by a second-order model which correlates well with data.

INTRODUCTION

Early work on turbulence modeling for wall-bounded flows with heat transfer is based on zero-equation models for the velocity field and the assumption of a constant Pr_t to relate $-\overline{u_i\theta}$ to $-\overline{u_iu_j}$. At a higher closure level, two-equation models or even second-order models have been used for the velocity field, while the assumption of a constant Pr_t is still invoked to model the turbulent heat fluxes [1]. Most of these approaches consist of using wall functions to bridge the gap between the region in which the model is valid and the wall. While this approach has been very successful for simple flows, it is not clear how to derive these wall functions for more complex flows. Furthermore, if the surface heat flux is to be evaluated properly, it is particularly important to have detailed knowledge of the velocity and temperature fields in the region very close to the wall. For simple flows, quite often, good agreement between these simple model calculations and data has been achieved for Pr near unity. For Pr departing from unity, however, Pr_t is found to depend on Pr [2]. No generally accepted correlation for Pr_t over a wide range of Pr has been found and this could be the result of the simple approach failing to capture the essential physics of the problem.

Recent direct numerical simulation (DNS) of wall turbulence with and without heat transfer shows that Pr_t is not constant across the flow field [3–5]. In order to relax the constant Pr_t assumption, several near-wall models have been proposed. These models solved the transport Reynolds equations for the velocity and temperature fields [6–8] with appropriate corrections made to allow them to integrate directly to the wall. The model of [6] is a full second-order closure based on the second-order velocity field model of [9], while the models of [7] and [8] are near-wall two-equation models solving for $\overline{\theta^2}$ and ε_θ and invoking a gradient transport assumption for the heat fluxes. Although these models are quite sucessful in general, certain deficiencies could still be identified. Among these are the inabilities of the models to predict flows with Pr significantly different from unity [6, 8], the incorrect asymptotic behavior calculated for the temperature field near a wall [7], the assumption of zero wall temperature fluctuations [6–8] and the inability to correctly predict the streamwise heat flux [7, 8]. Many practical flows of interest have Pr values significantly different from unity and various fluid–solid combinations will give rise to vastly different wall temperature fluctuations, especially in situations where heat transfer rates are high. Furthermore, in certain types of heat transfer problems and buoyant flows,

†Present address: ABB Power Generation Ltd, Gas Turbine Development, 5401 Baden, Switzerland.

NOMENCLATURE

b_{ij} Reynolds stress anisotropy tensor, $b_{ij} = \overline{u_i u_j}/(2k) - (1/3)\delta_{ij}$
C_f skin friction coefficient, $C_f = 2\tau_w/\rho U_m^2$
C_h heat transfer coefficient, $C_h = \bar{q}_w/\{\rho_\infty U_\infty c_p(\Theta_w - \Theta_{aw})\}$
D pipe diameter
D_{ij} production tensor, $D_{ij} = -\overline{u_i u_k}(\partial \bar{U}_k/\partial x_j) - \overline{u_j u_k}(\partial \bar{U}_k/\partial x_i)$
h channel half-width
H channel width
k turbulent kinetic energy
k^+ normalized turbulent kinetic energy, $k^+ = k/u_\tau^2$
Nu Nusselt number, $Nu = \bar{q}_w D(\Theta_w - \Theta_m)/(\rho c_p \alpha)$
n_i ith component of the unit normal vector positive outward from wall
$\tilde{P}$ production of k due to mean shear
P_{ij} production of Reynolds stresses due to mean shear, $P_{ij} = -\overline{u_i u_k}(\partial \bar{U}_j/\partial x_k) - \overline{u_j u_k}(\partial \bar{U}_i/\partial x_k)$
P_θ production of temperature variance due to mean temperature gradient, $P_\theta = -\overline{u_k \theta}(\partial \bar{\Theta}/\partial x_k)$
P_θ^* production of temperature variance due to streamwise mean temperature gradient
Pr Prandtl number
Pr_t turbulent Prandtl number
$\bar{q}_w$ mean wall heat flux
R time scale ratio, $R = (\overline{\theta^2}/\varepsilon_\theta)/(k/\varepsilon)$
Re Reynolds number based on bulk velocity, $Re = U_m D/\nu$ or $Re = U_m H/\nu$
Re_t turbulent Reynolds number, $Re_t = k^2/(\nu\varepsilon)$
Re_τ Reynolds number based on friction velocity, $Re_\tau = u_\tau h/\nu$ or $Re_\tau = u_\tau D/2\nu$
St Stanton number, $St = Nu/(RePr)$
$\bar{S}_{ij}$ mean strain rate tensor, $\bar{S}_{ij} = (1/2)(\partial \bar{U}_i/\partial x_j + \partial \bar{U}_j/\partial x_i)$
$\bar{U}_i$ ith component of the Reynolds averaged velocity
u_i ith component of the fluctuating velocity
U^+ mean velocity normalized with u_τ
U_m bulk mean velocity
u, v, w Reynolds fluctuating velocities along x-, y- and z-directions
u_τ friction velocity, $u_\tau = \sqrt{\tau_w/\rho}$
$-\overline{u_i u_j}$ Reynolds-stress tensor
$-\overline{u_i \theta}$ Reynolds-heat-flux vector
$-\overline{uv}^+$ normalized turbulent shear stress, $-\overline{uv}^+ = -\overline{uv}/u_\tau^2$
$-\overline{v\theta}^+$ normalized turbulent heat flux, $-\overline{v\theta}^+ = -\overline{v\theta}/(u_\tau \Theta_\tau)$
x_i ith component of the coordinate
x, y, z coordinates in streamwise, wall-normal and transverse directions
y^+ normalized wall-normal coordinate, $y^+ = y u_\tau/\nu$.

Greek symbols

α thermal diffusivity
α_t thermal eddy diffusivity
ε dissipation rate of k
$\tilde{\varepsilon}$ modified dissipation rate, $\tilde{\varepsilon} = \varepsilon - 2\nu(\partial\sqrt{k}/\partial y)^2$
$\bar{\varepsilon}$ modified dissipation rate, $\bar{\varepsilon} = \varepsilon - 2\nu k/y^2$
ε^+ normalized dissipation rate, $\varepsilon^+ = \varepsilon\nu/u_\tau^4$
ε_{ij} dissipation rate tensor
ε_θ dissipation rate of temperature variance, $\varepsilon_\theta = \alpha\overline{(\partial\theta/\partial x_k)(\partial\theta/\partial x_k)}$
$\tilde{\varepsilon}_\theta$ modified dissipation of temperature variance, $\tilde{\varepsilon}_\theta = \varepsilon_\theta - \alpha(\partial\sqrt{\overline{\theta^2}}/\partial y)^2$
ε_θ^* modified dissipation of temperature variance, $\varepsilon_\theta^* = \varepsilon_\theta - \alpha(\overline{\theta^2} - \overline{\theta_w^2})/y^2$
ν fluid kinematic velocity
ν_t eddy viscosity
$\bar{\Theta}$ Reynolds averaged temperature
Θ_m bulk mean temperature; $\Theta_m = \int \bar{U}\bar{\Theta}\,dA / \int \bar{U}\,dA$
Θ^+ normalized mean temperature, $\Theta^+ = (\bar{\Theta} - \Theta_w)/\Theta_\tau$
Θ_τ friction temperature, $\Theta_\tau = q_w/(\rho c_p u_\tau)$
θ fluctuating temperature
θ_{rms} root mean square of the temperature fluctuations, normalized with Θ_τ
$\overline{\theta^2}$ temperature variance
τ_w wall shear stress
ξ near-wall correction to ε equation
$\xi_{\varepsilon\theta}$ near-wall correction to ε_θ equation
$\bar{\omega}_{ij}$ mean rotation rate tensor, $\bar{\omega}_{ij} = (1/2)(\partial \bar{U}_i/\partial x_j - \partial \bar{U}_j/\partial x_i)$.

the streamwise heat flux plays an important role in determining the flow characteristics. Therefore, these deficiencies need to be addressed if practical problems in heat transfer are to be calculated correctly.

According to [10], where the performance of eight different near-wall second-order velocity field models against recent DNS data [11, 12] is analysed, only asymptotically correct models could yield predictions of the turbulence field similar to that given by the DNS data. Most important of all, if the near-wall model is not asymptotically correct, it would fail to yield a correct value for the von Karman constant, which is crucial to the prediction of wall-bounded flows. These conclusions are also found to be equally

applicable for two-equation models [13]. In view of these findings, the questions of near-wall asymptotic behavior and Pr dependence of the model are addressed simultaneously in [14]. A simple approach is adopted to remedy these two deficiencies in heat transfer modeling. The approach is based on the solution of the transport equations for $\overline{\theta^2}$ and ε_θ with suitable corrections made to the modeled equations to allow for proper asymptotic behavior near a wall. The heat fluxes are calculated using a simple thermal eddy diffusivity model. Furthermore, appropriate damping functions are introduced to account for variable Pr effects. Thus formulated, the model is quite successful in its predictions of pipe and channel flows with heat transfer spanning a Pr range from 0.01 to 10 000. Furthermore, the velocity and thermal von Karman constants are calculated correctly. In spite of these improvements, the model still invokes the assumption of $\theta = 0$ at the wall and essentially predicts a zero $\overline{u\theta}$ for all flow cases considered.

Most heat transfer calculations solve for the flow behavior in the fluid side only and seldom would an approach deal specifically with the conjugate problem, where there are interactions between the fluid and the solid wall. When the conjugate problem is solved, the conditions at the fluid–solid boundary are determined rather than specified. Attempts to solve for the true boundary conditions at the fluid–solid interface have been made [15, 16] and the results show that the boundary conditions are functions of the thermal activity ratio K and Pr. Except for a few special cases, the conjugate problem could not be easily solved because of limited computing power. Therefore, this limitation dictates that only the fluid side of a convective heat transfer problem could be simulated. If the solid side cannot be simulated, it is necessary to make assumptions on the thermal field at the wall. Usually, it is easier to invoke a reasonable physical assumption for the mean temperature; such as a constant wall temperature or a constant wall heat flux. The boundary condition for θ, on the other hand, is very difficult to determine. For the sake of convenience, it is usually assumed that θ vanishes at the wall. The effect of this idealized boundary condition on the calculated heat transfer characteristics in the near-wall region has been systematically analysed in [17]. It is found that Nu, St and other integral heat transfer properties are essentially not affected by assuming $\theta = 0$ at the wall. This assumption only affects the calculated $\overline{\theta^2}$ but not Θ in the near-wall region. Even then, all turbulence statistics outside of the near-wall region are not influenced by this idealized boundary condition. As a result, most of the deficiencies found in heat transfer modeling, except the inability of two-equation models to calculate $\overline{u\theta}$ correctly, have been addressed in one way or another.

Streamwise heat flux could be calculated fairly correctly using a second-order model [6]. It has been suggested [18] and verified [19] that correct heat transfer predictions could only be obtained using a temperature field model that is of lower or equal order compared to the velocity field model. In other words, at least a second-order velocity field model has to be used in conjunction with a second-order heat flux model. This could complicate the modeling problem immensely in the case of compressible and buoyant flows, because the uncoupled flow approximation [18] cannot be invoked. For three-dimensional flows, the total number of equations to be solved would include five mean flow equations, seven equations for $-\overline{u_iu_j}$ and ε, three equations for $-\overline{u_i\theta}$ and two equations for $\overline{\theta^2}$ and ε_θ. Aristotle once said, "It is the mark of an educated mind to rest satisfied with the degree of precision that the nature of the subject admits, and not to seek exactness when only an approximation is possible" (*Nicomachean Ethics*, 3rd century BC). In this spirit, the heat-flux model should be kept as simple as possible while still being able to reproduce the dominant physical effects. Therefore, it would be most expedient to seek a two-equation heat-flux model that could predict $\overline{u\theta}$ reasonably well compared to the second-order model. Such a model can be used with either a two-equation or a second-order velocity field model and substantial savings on computation time could result.

Algebraic models for the heat fluxes have been derived by various researchers [20–23]. The development usually follows the approach outlined in [24] for the development of an algebraic model for $-\overline{u_iu_j}$. The transport equation for $\overline{u_i\theta}$ is reduced to an algebraic equation by assuming that the convective and diffusive transport of $\overline{u_i\theta}$ is proportional to the transport of k and $\overline{\theta^2}$, which can be expressed as the difference between their respective production and dissipation rates. If, in addition, equilibrium turbulence is assumed, this equation can be further simplified and a linear system of equations for the vector $\overline{u_i\theta}$ is obtained. In solving this system of equations, a situation could occur where the matrix could become singular for certain combinations of $\overline{u_iu_j}$ and the mean gradients of U_i and Θ. This is similar to the singularity observed in [25] for algebraic Reynolds-stress models. Therefore, a straightforward application of these algebraic heat-flux models to wall shear flows may not be desirable.

These problems could be avoided if the model provides an explicit expression for $\overline{u_i\theta}$, i.e. they are expressible in terms of the known mean and turbulence fields. One such model has been developed [26] using statistical results from a two-scale direct-interaction approximation. However, the model has only been applied to calculate air flows with heat transfer far from solid boundaries. It has not been extended to near-wall flows of fluids with different Pr [26]. In practical engineering applications, the ability to integrate the model to the wall is most crucial because it impacts directly on the evaluation of such parameters as C_f, Nu and St, which are of primary importance to the development of heat transfer management code for power plants, gas turbine engines

and other industrial systems with widely varying Pr. Therefore, it is practical to develop a heat-flux model that could be applied to near-wall flows for a wide range of Pr. An alternative to the model of [26] is offered by the application of the simple extended diffusivity hypothesis outlined in [27] to existing algebraic models to render them explicit in $\overline{u_i\theta}$. If the resultant heat-flux model is to be valid for near-wall flows, it would be expedient to modify a well tested near-wall model using the approach of [27].

Since a simple thermal eddy diffusivity model that is capable of predicting a wide range of wall shear flows with varying Pr has already been developed [14], the present study will concentrate on the development of an explicit algebraic heat-flux (EAHF) model that would correctly recover the expression for $\overline{v\theta}$ given by the near-wall model of [14]; hereafter called the Simple model. This way, all the near-wall corrections previously devised could be applied without modifications and an improved near-wall heat transfer model that could yield a correct estimate of $\overline{u\theta}$ would result. The development of this model relies on the hypothesis proposed in [27]. Thus formulated, it can be shown that the usual singularities encountered in the system of heat-flux equations could be avoided. Furthermore, for homogeneous turbulent flows with a uniform temperature gradient, the expressions for $\overline{u_i\theta}$ thus derived are essentially similar to those obtained by previous researchers [20–23, 26]. The model can be used in conjunction with any near-wall two-equation or Reynolds-stress models [10, 25] for the velocity field, thus greatly simplifying the numerical solution of heat transfer problems. It could be easily extended to compressible and buoyant flows without having to solve additional equations. The extension to buoyant flows has been attempted [28]. Therefore, this paper only considers the validation of the EAHF model against non-buoyant flows.

AN EXPLICIT ALGEBRAIC HEAT-FLUX MODEL

The development of the EAHF model starts with the high-Reynolds-number version of the heat-flux equations [6]. It can be written as

$$\frac{D\overline{u_i\theta}}{Dt} - D^{t}_{i\theta} = -\overline{u_iu_k}\frac{\partial\bar{\Theta}}{\partial x_k} - \overline{u_k\theta}\frac{\partial\bar{U}_i}{\partial x_k} - C_{1\theta}\frac{1}{\tau}\overline{u_i\theta} + C_{2\theta}\overline{u_k\theta}\frac{\partial\bar{U}_i}{\partial x_k} \quad (1)$$

where $D^{t}_{i\theta}$ is the transport of $\overline{u_i\theta}$ due to turbulent diffusion, τ is an appropriate time scale and $C_{1\theta}$ and $C_{2\theta}$ are model constants. In [6], only the velocity time scale is used in the modeling of $\overline{u_i\theta}$ even though it was suggested that both the thermal and velocity time scales are important and should be adopted [21]. Two different mixed time scales have been proposed by previous researchers; these are $\tau = \sqrt{[(k/\varepsilon)(\overline{\theta^2}/\varepsilon_\theta)]}$ [7, 14] and $\tau = (\varepsilon/k)(\overline{\theta^2}/\varepsilon_\theta^2)$ [8, 26]. To date, neither of the two time scales has been shown to be clearly superior to the other one. However, it will be seen later that the use of $\tau = \sqrt{[(k/\varepsilon)(\overline{\theta^2}/\varepsilon_\theta)]}$ allows the expression of $\overline{v\theta}$ deduced from the Simple model to be recovered; an expression shown to be quite valid for a variety of flows covering a wide range of Re and Pr [14]. For this reason, $\tau = \sqrt{[(k/\varepsilon)(\overline{\theta^2}/\varepsilon_\theta)]}$ seems to be a more suitable choice for the present study.

Using the assumption of similarity between the transport of $\overline{u_i\theta}$ and the transport of k and $\overline{\theta^2}$, the left-hand side of (1) can be approximated by [24]

$$\frac{D\overline{u_i\theta}}{Dt} - D^{t}_{i\theta} = \frac{\overline{u_i\theta}}{k}(\tilde{P}-\varepsilon) + \frac{\overline{u_i\theta}}{\theta^2}(2P_\theta - 2\varepsilon_\theta). \quad (2)$$

If equilibrium turbulence for both the velocity and the thermal field is assumed, the right hand side of (2) becomes zero. Hence, the transport of $\overline{u_i\theta}$ can be neglected in (1) compared to other terms in the equation. Equation (1) can therefore be simplified to

$$-\overline{u_i\theta} = \frac{1}{C_{1\theta}}\sqrt{\left(\frac{k}{\varepsilon}\frac{\overline{\theta^2}}{\varepsilon_\theta}\right)}\left(\overline{u_iu_k}\frac{\partial\bar{\Theta}}{\partial x_k} + (1-C_{2\theta})\overline{u_k\theta}\frac{\partial\bar{U}_i}{\partial x_k}\right) \quad (3)$$

which constitutes a linear system of alegbraic equations for $\overline{u_i\theta}$.

So far, the derivation follows the classical approach. It should be pointed out that (3) gives an implicit expression for $\overline{u_i\theta}$ and singularities could occur for certain behavior of $\overline{u_iu_j}$ and the mean gradients of U_i and Θ. Therefore, a different approach is required to remedy this situation. The expression can be made explicit by using a successive approximation method. In other words, simple gradient transport models are assumed for $\overline{u_iu_j}$ and $\overline{u_i\theta}$ on the right-hand side of (3). This is equivalent to taking the first approximation in the expansions for a gradient transport representation of $\overline{u_iu_j}$ and $\overline{u_i\theta}$ in the evaluation of (3). Assuming simple gradient transport models for $\overline{u_iu_j}$ and $\overline{u_i\theta}$ [13, 14] to be given by

$$-\overline{u_iu_k} = \nu_t\left(\frac{\partial\bar{U}_i}{\partial x_k} + \frac{\partial\bar{U}_k}{\partial x_i}\right) - \tfrac{2}{3}\delta_{ik}k \quad (4)$$

$$-\overline{u_i\theta} = \alpha_t\frac{\partial\bar{\Theta}}{\partial x_i} \quad (5)$$

the resulting equation, after re-arrangement, takes the form

$$-\overline{u_i\theta} = \frac{2}{3C_{1\theta}}k\sqrt{\left(\frac{k}{\varepsilon}\frac{\overline{\theta^2}}{\varepsilon_\theta}\right)}\frac{\partial\bar{\Theta}}{\partial x_i} - \frac{1}{C_{1\theta}}\sqrt{\left(\frac{k}{\varepsilon}\frac{\overline{\theta^2}}{\varepsilon_\theta}\right)} \times ((2\nu_t + (1-C_{2\theta})\alpha_t)\bar{S}_{ik} + (1-C_{2\theta})\alpha_t\bar{\omega}_{ik})\frac{\partial\bar{\Theta}}{\partial x_k} \quad (6)$$

where the strain rate tensor $\bar{S}_{ij}$ and the rotation rate tensor $\bar{\omega}_{ij}$ are used. These notations were first introduced in [24] and later adopted in [25, 26]. The eddy diffusivities are given by

$$\nu_t = c_\mu f_\mu \frac{k^2}{\varepsilon} \tag{7a}$$

$$\alpha_t = c_\lambda f_\lambda k \left(\frac{k}{\varepsilon} \frac{\overline{\theta^2}}{\varepsilon_\theta} \right)^{1/2} \tag{7b}$$

where the damping functions f_μ and f_λ are introduced to allow direct integration of the model to the wall in order to satisfy the asymptotic behavior of the turbulence statistics in the near-wall region [13, 14]. It can be seen that the form of this equation is similar to the extended thermal eddy diffusivity model proposed in [27], i.e.

$$-\overline{u_i\theta} = D_{ij}^{\mathrm{B}} \frac{\partial \bar{\Theta}}{\partial x_j}. \tag{8}$$

The components of D_{ij}^{B} are determined by comparing coefficients between (6) and (8).

Thus formulated, the first term in (6) is affected by both the velocity and the temperature time scales and is similar to the Simple model given in (7b). The second term gives a non-zero turbulent heat flux in the streamwise direction even when there is no streamwise temperature gradient. In other words, consistent with the thermal physics, the turbulent eddies generate a $\overline{u\theta}$ due to their interactions with the mean temperature gradient normal to the streamwise direction. It can be seen that the modeled equation for $\overline{u_i\theta}$ derived here is always regular. Therefore, the approximations also allow the numerical difficulties to be avoided.

If (6) is used to calculate the heat fluxes for flows where the thin shear layer approximation holds, the result for $\overline{v\theta}$ is of the same form as that given in (5), or

$$-\overline{v\theta} = \frac{2}{3C_{1\theta}} k \sqrt{\left(\frac{k}{\varepsilon} \frac{\overline{\theta^2}}{\varepsilon_\theta} \right)} \frac{\partial \bar{\Theta}}{\partial y} \tag{9}$$

while the result for $\overline{u\theta}$ is given by

$$-\overline{u\theta} = \frac{2}{3C_{1\theta}} k \sqrt{\left(\frac{k}{\varepsilon} \frac{\overline{\theta^2}}{\varepsilon_\theta} \right)} \frac{\partial \bar{\Theta}}{\partial x} - \frac{1}{C_{1\theta}} \sqrt{\frac{k}{\varepsilon} \frac{\overline{\theta^2}}{\varepsilon_\theta}} \times \left((\nu_t + (1 - C_{2\theta})\alpha_t) \frac{\partial \bar{U}}{\partial y} \right) \frac{\partial \bar{\Theta}}{\partial y}. \tag{10}$$

The first term on the right-hand side of (10) is equivalent to that given by the Simple model while the second term represents an improvement to the estimate of $\overline{u\theta}$. Since the streamwise temperature gradient is small in channel/pipe and boundary-layer flows, the first term alone cannot determine $\overline{u\theta}$ properly. With the addition of the second term, which relates $\overline{u\theta}$ to the cross-stream temperature gradient, an improved estimate can be obtained. Note that if (3) is solved directly for the case of channel flows, thus leading to a classical algebraic model, the results yield explicit expressions for $\overline{u\theta}$ and $\overline{v\theta}$. For this special case, the singularities mentioned above are not present. Only for truly two- or three-dimensional problems would they occur. It should be pointed out that, if the small terms due to the streamwise temperature gradient are neglected, the channel flow results yield very similar expressions for both $\overline{u\theta}$ and $\overline{v\theta}$ compared to (9) and (10). In particular, (9) could be interpreted as a simplified version of the channel flow result assuming isotropic Reynolds stresses.

The model constants $C_{1\theta}$ and $C_{2\theta}$ have not been specified. If the values, $C_{1\theta} = 3$ and $C_{2\theta} = 0.4$, adopted in [6] are used in the present formulation, the Simple model could not be recovered correctly. Part of the reason could be due to the fact that in [6] only the velocity time scale is used in the modeled equation. In order to obtain the equivalent constant for the mixed time scale used here, the constant $C_{1\theta}$ has to be divided by $\sqrt{(2R)}$. According to [29], $R \approx 0.6$ for flows with $Pr = 0.71$. If this value of R is used to calculate $C_{1\theta}$, a value $C_{1\theta} = 3.28$ is obtained. Furthermore, if the constant coefficient in (9) is taken to be the constant c_λ and $f_\lambda = 1$ is assumed as in the Simple model, a value of $c_\lambda = 0.203$ is determined. However, it should be pointed out that the term $\overline{v^2}$ appears in the relation for $\overline{v\theta}$ derived from (3) instead of $2/3k$ appearing in (9). For wall shear flows $\overline{v^2} \approx 1/3k$ [11], therefore, an extra factor of about two appears in (9). In order to recover the Simple model correctly, the constant $2/(3C_{1\theta})$ in the first term of the right-hand side of (6), (9) and (10) is replaced by $c_\lambda \approx 0.095$, while $C_{1\theta} = 3.28$ is retained in the second term. The value of $C_{2\theta}$ in (6) can be adopted without modification from [6] as $C_{2\theta} = 0.4$.

With this choice of model constants, the expression for $\overline{v\theta}$ is identical to that given by the Simple model, therefore, the near-wall corrections used in that model can be adopted without change. This means that the coefficient $(2/3C_{1\theta})k[(k/\varepsilon)(\overline{\theta^2}/\varepsilon_\theta)]^{1/2}$ in (9) and (10) should be replaced by α_t. With this substitution and the near-wall damping functions given in [13, 14], the EAHF model in its final form can be written as

$$-\overline{u_i\theta} = \alpha_t \frac{\partial \bar{\Theta}}{\partial x_i} - \frac{1}{C_{1\theta}} \sqrt{\left(\frac{k}{\varepsilon} \frac{\overline{\theta^2}}{\varepsilon_\theta} \right)} \times \{ [2\nu_t + (1 - C_{2\theta})\alpha_t] \bar{S}_{ik} + (1 - C_{2\theta})\alpha_t \bar{\omega}_{ik} \} \frac{\partial \bar{\Theta}}{\partial x_k} \tag{11}$$

where α_t and ν_t are given by equations (7a) and (7b), respectively. In this final form, (11) with $C_{1\theta} = 3.28$ and $C_{2\theta} = 0.4$ is very similar to a scalar flux model derived by Yoshizawa [26]. The main advantage of (11) is that it is straightforward to derive. Furthermore, the model recovers the expression for $\overline{v\theta}$ as given by the Simple model which has been validated against flows with heat transfer covering a wide range of Re and Pr. However, the major differences between (11) and that given in [26], besides the fact that (11) represents a near-wall model, lie in the model constants and the time scales adopted. This way of deriving the model and determining the constants may not be very rigorous, but its similarity to Yoshizawa's

expression shows that the present approach used to derive (11) is sound.

The damping functions associated with α_t and ν_t are quoted here as

$$f_\lambda = (1-f_{\lambda 1})\frac{C_{\lambda 1}}{Re_t^{1/4}} + f_{\lambda 1} \tag{12}$$

$$f_{\lambda 1} = [1-\exp(-y^+/A^+)]^2 \tag{13}$$

$$f_\mu = \left(1+\frac{3.45}{\sqrt{Re_t}}\right)\tanh\left(\frac{y^+}{115}\right) \tag{14}$$

where $C_{\lambda 1} = 0.4/Pr^{1/4}$ for $Pr < 0.1$, $C_{\lambda 1} = 0.7/Pr$ for $Pr \geqslant 0.1$ and $A^+ = 10/Pr$ for $Pr < 0.25$, $A^+ = 39/Pr^{1/16}$ for $Pr \geqslant 0.25$ are adopted because they have been shown to yield excellent predictions for a wide range of Re and Pr and for different wall thermal boundary conditions [14]. With this formulation, $\overline{u\theta}$ does not exhibit the proper near-wall behavior of y^2. This could not be achieved without the introduction of even more damping functions. Since $\overline{v\theta}$ still dominates wall shear flows, an incorrect asymptotic behavior of $\overline{u\theta}$ in the near-wall region could be tolerated. Even so, the EAHF model provides a significant improvement to the prediction of $\overline{u\theta}$; allowing the proper order of magnitude to be estimated under the condition where the streamwise gradient of Θ is approximately zero.

THE MODELED EQUATIONS

Channel and pipe flow experiments are used to validate the proposed model. Consequently, the governing equations in their respective physical coordinates are rather simple and are fairly easy to deduce from the tensor equations. Therefore, in the following, only the modeled equations are given. The near-wall Reynolds-stress model of [30] is used to calculate the velocity field while the near-wall two-equation model of [14] is adopted for the calculation of $\overline{\theta^2}$ and ε_θ. These modeled equations, in Cartesian tensor form, are quoted here for reference, or

$$\frac{D\overline{u_iu_j}}{Dt} = \frac{\partial}{\partial x_k}\left(\nu\frac{\partial\overline{u_iu_j}}{\partial x_k}\right) + D_{ij}^T - \left(\overline{u_iu_k}\frac{\partial\bar{U}_j}{\partial x_k} + \overline{u_ju_k}\frac{\partial\bar{U}_i}{\partial x_k}\right) + \Pi_{ij} - \varepsilon_{ij} \tag{15}$$

$$\frac{D\varepsilon}{Dt} = \frac{\partial}{\partial x_k}\left(\nu\frac{\partial\varepsilon}{\partial x_k}\right) + \frac{\partial}{\partial x_i}\left(C_\varepsilon\frac{k}{\varepsilon}\overline{u_iu_j}\frac{\partial\varepsilon}{\partial x_j}\right) + C_{\varepsilon 1}\frac{\varepsilon}{k}\tilde{P} - C_{\varepsilon 2}\frac{\tilde{\varepsilon}}{k}\varepsilon + \xi \tag{16}$$

$$\frac{D\overline{\theta^2}}{Dt} = \frac{\partial}{\partial x_k}\left(\alpha\frac{\partial\overline{\theta^2}}{\partial x_k}\right) + \frac{\partial}{\partial x_k}\left(C_{\theta^2}\frac{k}{\varepsilon}\overline{u_ku_j}\frac{\partial\overline{\theta^2}}{\partial x_j}\right) - 2\overline{u_j\theta}\frac{\partial\bar{\Theta}}{\partial x_j} - 2\varepsilon_\theta \tag{17}$$

$$\frac{D\varepsilon_\theta}{Dt} = \frac{\partial}{\partial x_k}\left(\alpha\frac{\partial\varepsilon_\theta}{\partial x_k}\right) + \frac{\partial}{\partial x_k}\left(C_{\varepsilon_\theta}\frac{k}{\varepsilon}\overline{u_ku_j}\frac{\partial\varepsilon_\theta}{\partial x_j}\right) + C_{d1}\frac{\varepsilon_\theta}{\overline{\theta^2}}P_\theta + C_{d2}\frac{\varepsilon}{k}P_\theta + C_{d3}\frac{\varepsilon_\theta}{k}\tilde{P} - C_{d4}\frac{\tilde{\varepsilon}_\theta}{\overline{\theta^2}}\varepsilon_\theta - C_{d5}\frac{\tilde{\varepsilon}}{k}\varepsilon_\theta + \xi_{\varepsilon_\theta} \tag{18}$$

$$D_{ij}^T = \frac{\partial}{\partial x_k}\left\{C_s\frac{k}{\varepsilon}\left(\overline{u_iu_l}\frac{\partial\overline{u_ju_k}}{\partial x_l} + \overline{u_ju_l}\frac{\partial\overline{u_ku_i}}{\partial x_l} + \overline{u_ku_l}\frac{\partial\overline{u_iu_j}}{\partial x_l}\right)\right\} \tag{19}$$

$$\Pi_{ij} = -C_1(1-f_{w1})\frac{\varepsilon}{k}(\overline{u_iu_j} - \tfrac{2}{3}\delta_{ij}k) - (\alpha_1 - \alpha^* f_{w1})(P_{ij} - \delta_{ij}\tilde{P}) - \beta_1(D_{ij} - \delta_{ij}\tilde{P}) - 2\left(\gamma_1 - C_w\frac{k^{3/2}}{\varepsilon y}\right)k\bar{S}_{ij} - f_{w1}\frac{\varepsilon}{k}(\overline{u_iu_k}n_kn_j + \overline{u_ju_k}n_kn_i) \tag{20}$$

$$\varepsilon_{ij} = \tfrac{2}{3}(1-f_{w1})\varepsilon\delta_{ij} + f_{w1}\frac{\varepsilon}{k} \times \frac{\overline{u_iu_j} + \overline{u_iu_k}n_kn_j + \overline{u_ju_k}n_kn_i + n_in_j\overline{u_ku_l}n_kn_l}{1 + 3\overline{u_ku_l}n_kn_l/2k} \tag{21}$$

$$\xi = f_{w2}\left(1.5\frac{\tilde{\varepsilon}^2}{k} - 2\frac{\varepsilon\tilde{\varepsilon}}{k} - 1.5C_{\varepsilon 1}\tilde{P}\right) \tag{22}$$

$$\xi_{\varepsilon_\theta} = f_{w,\varepsilon_\theta}\left((C_{d4}-4)\frac{\tilde{\varepsilon}_\theta}{\overline{\theta^2}}\varepsilon_\theta + C_{d5}\frac{\tilde{\varepsilon}}{k}\varepsilon_\theta - \frac{\varepsilon_\theta^{*2}}{\overline{\theta^2}} + (2 - C_{d1} - PrC_{d2})\frac{\varepsilon_\theta}{\overline{\theta^2}}P_\theta^*\right). \tag{23}$$

The damping functions $f_{w1} = \exp[-(Re_t/150)^2]$, $f_{w2} = \exp[-(Re_t/40)^2]$ and $f_{w,\varepsilon_\theta} = \exp[-(Re_t/80)^2]$ are introduced to ensure that the near-wall corrections would go to zero far away from a wall and the model constants C_ε, $C_{\varepsilon 1}$, $C_{\varepsilon 2}$, C_{θ^2}, C_{ε_θ}, C_{d1}, C_{d2}, C_{d3}, C_{d4}, C_{d5}, C_s, C_1, C_2, α_1, α^*, β_1, γ_1 are specified as 0.10, 1.50, 1.83, 0.11, 0.11, 1.80, 0, 0.72, 2.20, 0.80, 0.11, 3.0, 0.4, 0.7636, 0.45, 0.1091, 0.1818, respectively. On the other hand, the modified dissipation rates, $\bar{\varepsilon} = \varepsilon - 2\nu k/y^2$ and $\tilde{\varepsilon} = \varepsilon - 2\nu(\partial\sqrt{k}/\partial y)^2$, are introduced to render the ε-equation regular as a wall is approached. Wall reflection effects are also modeled in (20) and this gives $C_w = -0.00805 + 0.00519 \cdot \ln(Re)$ for pipe and channel flows. Finally, the mean flow boundary conditions are no slip at the wall and constant wall heat flux or constant wall temperature, while the boundary conditions at y = 0 for the turbulence field are given by $\overline{u_iu_j} = \overline{\theta^2} = 0$, $\varepsilon_w = 2\nu(\partial\sqrt{k}/\partial y)^2$ and $(\varepsilon_\theta)_w = (\alpha/2)(\partial^2\overline{\theta^2}/\partial y\,\partial y)$.

The equations for fully-developed flows are ordinary differential equations. They are relatively easy to solve using existing numerical algorithms. In the present study, these equations are solved using a simple relaxation method [9]. Iterations based on an initial guess for the velocity and temperature fields are

carried out to obtain a convergent solution to the governing equations. A parabolic code [31] is used to calculate entrance flow in a pipe or channel. The entrance flows to be calculated have a fully-developed velocity field. Therefore, inlet conditions for the velocity field are simply specified from a previous run that has achieved a fully-developed state. On the other hand, the inlet conditions for the thermal field are more difficult to specify. The following procedure is adopted here after numerous experiments. A constant mean temperature is assumed, while $\overline{\theta^2}$ and ε_θ are calculated by $\overline{\theta^2}^{++} = k^+$ and $\varepsilon_\theta^{++} \approx 0.5\varepsilon^+$. The dimensional values at the inlet are then obtained by setting $\overline{\theta^2} = \overline{\theta^2}^{++}\Theta_\tau^{++2}$ and $\varepsilon_\theta = \varepsilon_\theta^{++}\Theta_\tau^{++2}u_\tau^2/\nu$ where Θ_τ^{++} is the friction temperature Θ_τ divided by a factor ranging from 50 to ~ 100. Various tests show that the exact value of this factor only exerts an insignificant influence on the results.

MODEL VALIDATION

The major improvement in the present model is the prediction of $\overline{u\theta}$. Therefore, it is necessary to validate this prediction against a variety of data. The calculations are validated against DNS data [3, 5] and experimental measurements [32–34]. In addition to these calculations, entrance flow heat transfer is also carried out for a wide range of *Re*. Streamwise heat flux affects the development of *Nu* and the centerline temperature in the thermal entrance region. If $\overline{u\theta}$ is not calculated correctly, the predictions of the centerline temperature and *Nu* will also be in error. Therefore, it is important to verify the model against this type of flow. The calculations are compared with experimental measurements [34–36]. In addition, whenever data are available, the calculations are also compared with the evolution of the mean temperature field in the entrance region.

Since the EAHF model yields the same expression for $\overline{v\theta}$ as the Simple model, the calculated Θ, $\overline{\theta^2}$ and $\overline{v\theta}$ are hardly affected by the improved model for $\overline{u\theta}$. This is obvious from the mean temperature equation and the fact that the expression for $\overline{v\theta}$ is exactly the same as that given by the Simple model. A major difference occurs in the production of $\overline{\theta^2}$ due to the streamwise temperature gradient. However, this term is still small compared to the production due to normal temperature gradient. As a result, the prediction of $\overline{\theta^2}$ is essentially unchanged compared to the previous results [14]. Some results are shown here to demonstrate that these quantities are little affected. The remaining comparisons are made with $\overline{u\theta}$ only.

The first comparisons are made with DNS data obtained from fully-developed channel flows at $Re = 5600$ [3] and $Re = 4560$ [5]. Predictions based on the Reynolds-stress model for the velocity field and both the EAHF and Simple model for the temperature field are compared with the data of [5], while only the EAHF model calculations are compared with the data of [3]. The comparisons with the DNS data of [5] at

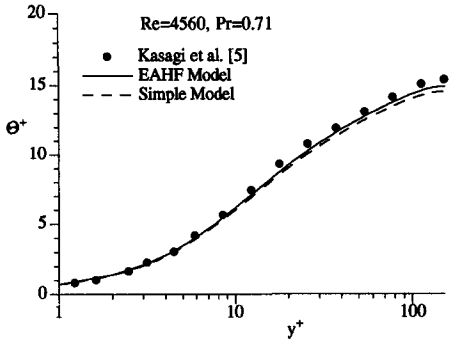

Fig. 1. Comparison of calculated mean temperature with DNS data.

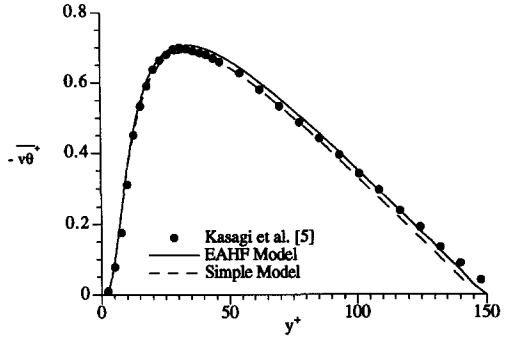

Fig. 2. Comparison of the calculated normal heat flux with DNS data.

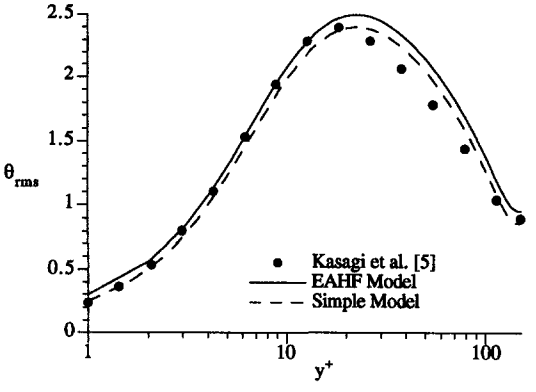

Fig. 3. Comparison of the calculated rms temperature variance with DNS data.

$Pr = 0.71$ are shown in Figs. 1–4, while those with the data of [3] at $Pr = 0.1$, 0.71 and 2.0 are given in Fig. 5. These comparisons show that Θ (Fig. 1), $\overline{v\theta}$ (Fig. 2) and $\overline{\theta^2}$ (Fig. 3) are essentially not affected by the EAHF model. There is a very slight difference between the two model calculations though. The smallest difference occurs in the prediction of Θ, while $\overline{\theta^2}$ shows the greatest change. In any case, the differences are small and are not enough to significantly influence the calculated *Nu* and *St*.

The Simple model essentially yields a zero prediction for $\overline{u\theta}$. In contrast, the prediction of $\overline{u\theta}$ by the

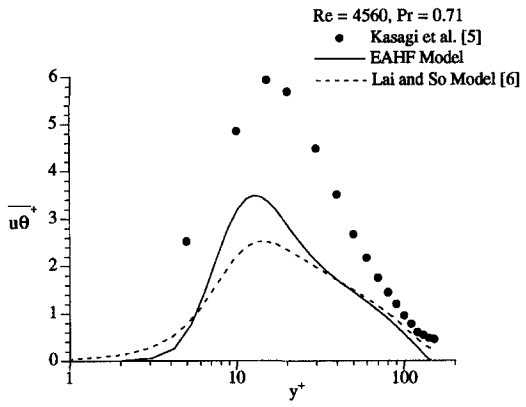

Fig. 4. Comparison of calculated streamwise heat flux with DNS data.

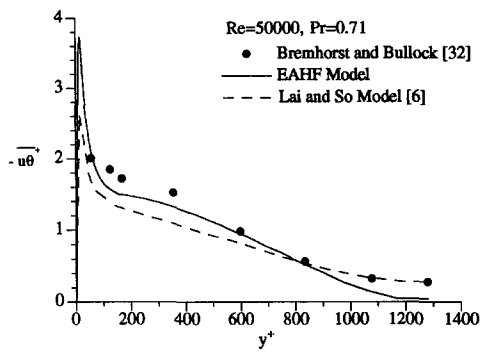

Fig. 6. Comparison of calculated streamwise heat flux with measurements.

EAHF model is vastly improved even though the peak values are substantially underpredicted (Figs. 4 and 5). It seems that this under-prediction is a function of Re and Pr. At $Pr = 0.1$, the EAHF model yields a fairly correct prediction of $\overline{u\theta}$ (Fig. 5). The DNS cases considered here have very low Re, therefore, the assumption of equilibrium turbulence invoked to deduce (3) is not quite valid. It is reasonable to expect that the agreement between predictions and measurements would improve as Re increases; see later comparisons (Figs. 6 and 7). There is also a rather large discrepancy between the predicted $\overline{u\theta}$ and the DNS data near the pipe center. Overall, the EAHF model yields a prediction of $\overline{u\theta}$ close to the calculation of the second-order model of [9]. The second-order model performs better near the centerline because the EAHF model predicts a zero value for $\overline{u\theta}$ as a result of the gradient transport assumption even though experimental measurements show that $\overline{u\theta}$ at this location is non-zero. If a possible near-wall extension of the model of [26] is used to calculate the DNS data, the same discrepancies could be expected. The reason is that Yoshizawa's [26] model is similar to that given by (11) except that the model constants and time scales adopted are different. Changing the model constants could change the peak values calculated for $\overline{u\theta}$, but they will also affect the predictions of other quantities such as Θ, $\overline{\theta^2}$ and $\overline{v\theta}$. As for changing the time scales, the effects are nonlinear and the calculations could lead to quite different results altogether. Finally, the comparisons with the pipe flow experiment [34] are not shown because the calculated differences between the EAHF model and the Simple model are essentially identical to those plotted in Figs. 1–3. Furthermore, these results have been previously reported [13, 14].

Further streamwise heat flux comparison (Fig. 6) is carried out with fully-developed pipe flow measurements [32] at $Re = 50\,000$ and the second-order model of [9]. No comparison is made in the immediate near-wall region because of the rather coarse resolution of the experimental data. Over most of the flow field, the prediction of the EAHF model is in better agreement with data than that of the second-order model. The difference between the two calculated results is, however, relatively small except, again, near the centerline. Note that the EAHF model predicts a larger peak value of $\overline{u\theta}$ compared to the second-order model. A final comparison is carried out with the fully-developed pipe flow measurements of [33] at $Re = 40\,000$. The EAHF model is able to correctly

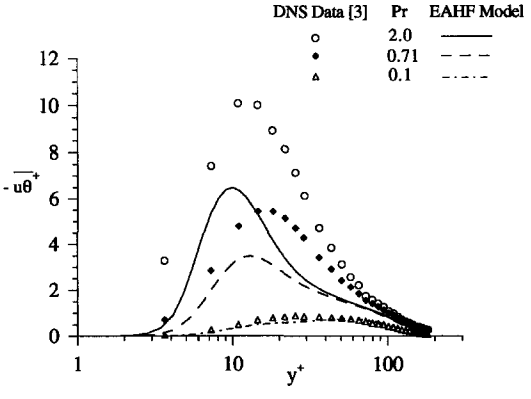

Fig. 5. Comparison of calculated streamwise heat flux with DNS data.

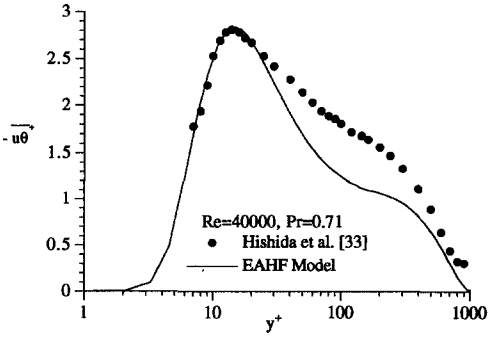

Fig. 7. Comparison of calculated streamwise heat flux with measurements.

predict the magnitude as well as the location of the peak in $\overline{u\theta}$ (Fig. 7). Over most of the flow field, the prediction is in fair agreement with data. Near the centerline, the model again yields a vanishing heat flux while the data shows a small, but non-zero value. On the other hand, the Simple model gives a $\overline{u\theta}$ that is essentially zero across most of the pipe. The largest calculated value of $-\overline{u\theta}^+ = 0.015$ occurs at the pipe center. Even then, it is more than one order of magnitude smaller than the measured value of about 0.3. This clearly shows the great improvement due to the EAHF model. Calculations of other fully-developed pipe flow measurements [34] with $Re = 71\,200$ and $Pr = 0.71$ have also been made. Data on $\overline{u\theta}$ are not available. The calculations are compared with the measured Θ and $\overline{v\theta}$ only. Results obtained are similar to those shown in Figs. 1 and 2. Therefore, the comparisons are not reported here.

Calculations up to this point are performed using the Reynolds-stress model of [30] where C_w depends on Re. This constant is introduced as the coefficient of a term to model wall reflection effects. The wall reflection term introduces a new length scale into the Reynolds-stress model. This length scale may be appropriate for cases in which the temperature can be regarded as a passive scalar. In other words, for the above calculations, the wall-reflection term would not present a major problem. However, for flows with high heat transfer rates and buoyant and compressible flows, the length scale imposed by the wall-reflection term could lead to poor results. After all, this term is introduced to ensure that the near-wall Reynolds-stress model would reproduce the log-law region of the velocity field correctly. In buoyant flows, the extent of the log-law region is modified by buoyancy effects. For flows with high Froude numbers, the log-law region could disappear entirely [37]. A wall reflection term that enforces a log-law region would thus lead to poor results. Recently, a new near-wall Reynolds-stress model based on the quasi-linear pressure-strain model of [38] has been formulated and validated [31]. One major advantage of the new model is that the log-law region is calculated correctly without a wall reflection term. Therefore, it is better suited for more complex flows. In view of this, the thermal entrance flow calculations are carried out using this new near-wall model [31]. Another reason for this change is to verify that the EAHF model is not unduely affected by the choice of the velocity field models as long as they are of the same closure level. This new model combination has been validated against some of the simple flows discussed above and the same results as before are obtained.

The only difference between the near-wall Reynolds-stress closure of [31] and that of [30] is in the modeling of the pressure strain tensor. As a result of this modification, the model constants in (20) and (22) are changed slightly. For completeness sake, the model terms for Π_{ij} and ξ are listed below. They are given by

$$\begin{aligned}\Pi_{ij} = &-(2C_1\varepsilon + C_1^*\tilde{P})(1-f_{w1})b_{ij} + C_2(1-f_{w1})\\ &\times\varepsilon(b_{ik}b_{kj} - \tfrac{1}{3}\delta_{ij}\Pi)\\ &-(\alpha_1 - \alpha^* f_{w1})(P_{ij} - \delta_{ij}\tilde{P}) - \beta_1(D_{ij} - \delta_{ij}\tilde{P})\\ &-2\left(\gamma_1 - f_{w1}\gamma^* + \frac{C_3^*}{2}\Pi^{1/2}\right)k\bar{S}_{ij}\\ &-\frac{1}{3}\left(\frac{\partial}{\partial x_m}\left(\nu\frac{\partial\overline{u_i u_k}}{\partial x_m}\right)n_k n_j + \frac{\partial}{\partial x_m}\left(\nu\frac{\partial\overline{u_j u_k}}{\partial x_m}\right)n_k n_i\right)\\ &+\frac{1}{3}\frac{\partial}{\partial x_m}\left(\nu\frac{\partial\overline{u_k u_p}}{\partial x_m}\right)n_k n_p n_i n_j \end{aligned} \tag{24}$$

$$\xi = f_{w2}\left(-L\frac{\varepsilon}{k}\tilde{P} + M\frac{\tilde{\varepsilon}^2}{k} - N\frac{\varepsilon\tilde{\varepsilon}}{k}\right) \tag{25}$$

where the model constants different from those given above are specified in [38] as C_1, C_2, C_1^*, C_3^*, α_1, α^*, β_1, γ_1, γ^*, L, M, N, equal to 3.4, 4.2, 1.8, 1.3, 0.4125, −0.29, 0.2125, 0.01667, 0.065, 2.25, 0.5, 0.57, respectively, $f_{w1} = \exp[-(Re_t/200)^2]$ and f_{w2} remain the same.

The comparisons of the calculated Nu with measurements [35, 36] are shown in Fig. 8. In general, the Nu behavior is reproduced quite well. The only significant difference occurs in the region very close to the entrance of the heated section, where x is taken to be zero. The final asymptotic values of Nu correlate well with measurements even though the largest discrepancy occurring at $Re = 71\,000$ is about 10%. Note that only the heat transfer coefficient C_h and the pipe diameter D are reported in [35]. Therefore, the thermal conductivity ($\alpha\rho c_p$) had to be estimated. Since the temperature for $Re = 71\,000$ is not given, there could be some error introduced in the estimate of Nu. On the other hand, Nu is reported directly in [36] and the agreement between calculation and data is very good beyond about one diameter downstream of the entrance to the heated section. The calculated centerline temperature is compared with data for three cases

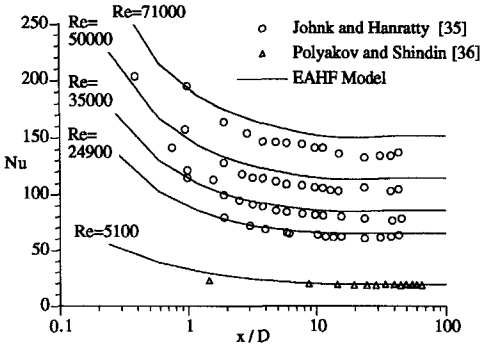

Fig. 8. Comparison of the calculated Nu in the thermal entrance region with measurements.

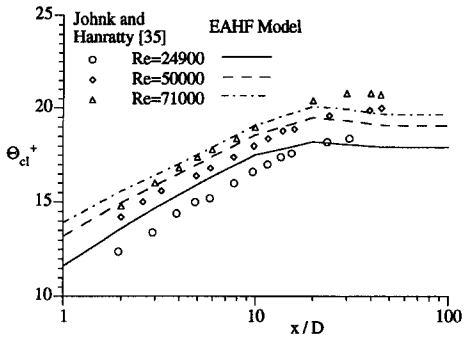

Fig. 9. Comparison of the calculated centerline temperature in the thermal entrance region with measurements.

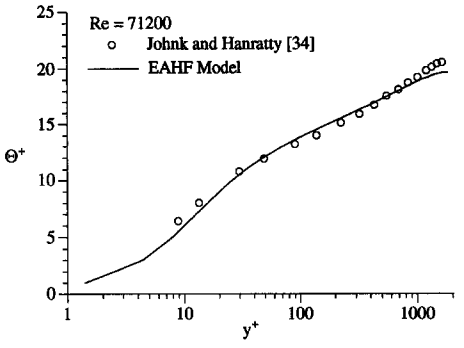

Fig. 11. Mean temperature comparison in a fully-developed pipe flow.

at high Reynolds numbers (Fig. 9). Again, agreement with data is reasonable with the largest errors occurring in the region near the entrance to the heated section.

The reason for the discrepancy near the entrance to the heated section could be due to the uncertainty in the estimate of the inlet conditions as well as the fact that the parabolic assumption is strictly not applicable at this location. Therefore, the virtual origin of the thermal boundary layer of the experiments is not necessarily coincident with that assumed for the calculations. For this reason, the comparisons of the temperature profiles in Fig. 10 are carried out by requiring that the calculated and measured temperature profiles be in agreement at the first experimental station. Thus determined, the virtual origin is found to be at $x/D = 0.31$ downstream of the entrance to the heated section. After this adjustment, the calculated mean temperature profiles are in good agreement with data at each location. This means that, with the exception of the region within less than one diameter, the EAHF model correctly predicts the evolution of the thermal field. Beyond $x/D = 40$, the temperature field becomes fully developed and the fully-developed temperature profile (Fig. 11) recovered is essentially identical to that obtained using the model of [30] to calculate the velocity field. Therefore, the EAHF model is fairly independent of the choice of velocity models used.

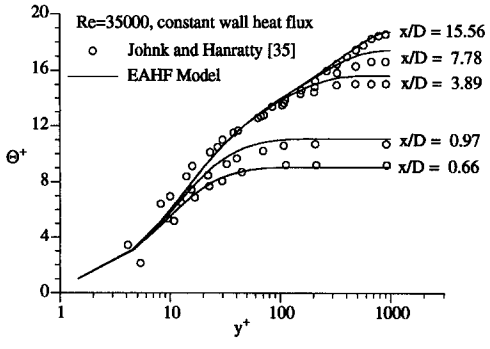

Fig. 10. Comparison of the calculated centerline temperature profiles in the thermal entrance region with measurements.

CONCLUSIONS

An explicit algebraic heat-flux (EAHF) model has been derived for the calculation of the turbulent temperature field. The derivation invokes equilibrium turbulence to reduce the transport equations to a system of linear equations and the final EAHF model is obtained by adopting a simple approximation concept proposed by Batchelor [27]. Analysis of the model shows that the same near-wall damping functions as given in the Simple model can be used to obtain an asymptotically correct near-wall behavior for $\overline{v\theta}$. As for $\overline{u\theta}$, no attempt has been made to obtain the correct asymptotic near-wall behavior because this would require the introduction of additional damping functions. Besides, this mismatch does not seem to have any significant effects on the thermal properties for all the flow cases tested.

The EAHF model is validated against fully developed channel and pipe flows and the calculations are compared with DNS data, experimental measurements and Simple and second-order model predictions. The governing equations show that there should be very little difference between the calculated Θ, $\overline{\theta^2}$ and $\overline{v\theta}$ obtained from the EAHF and the Simple model. This conclusion is essentially verified by the present calculations. Predictions of $\overline{u\theta}$, however, are much more realistic compared to the Simple model and are in much better agreement with data and the second-order model results. The best correlation with data is obtained at high Reynolds numbers and in the log layer. This is not surprising, since equilibrium turbulence is assumed in the derivation of the model. The importance of an improved prediction of $\overline{u\theta}$ is not obvious for simple flows, since it hardly changes Θ and the thermal turbulence quantities other than $\overline{u\theta}$. However, it is very important to the calculations of buoyant turbulent flows where $\overline{u\theta}$ can have a significant effect on the predicted thermal field. The results presented also show that the EAHF model performs well with two different near-wall Reynolds-stress model. In addition, the development of the temperature field in the thermal entrance region of a pipe flow at different Reynolds numbers is correctly calculated.

Acknowledgement—The authors wish to acknowledge the support given them by NASA Langley Research Center, Hampton, Virginia, under grant no. NAG-1-1080. The grant was monitored by Dr T. B. Gatski.

REFERENCES

1. H. K. Myong and N. Kasagi, Numerical prediction of turbulent pipe flow heat transfer for various Prandtl number fluids with the improved k–ε turbulence model, *JSME Int. J. Ser.* II **32,** 613–622 (1989).
2. M. Jischa and H. B. Rieke, About the prediction of turbulent Prandtl and Schmidt numbers from modeled transport equations, *Int. J. Heat Mass Transfer* **22,** 1547–1555 (1979).
3. J. Kim and P. Moin, Transport of passive scalars in a turbulent channel flow, *Turbulent Shear Flows* **6,** 85–96 (1989).
4. S. L. Lyons, T. J. Hanratty and J. B. McLaughlin, Direct numerical simulation of passive heat transfer in a turbulent channel flow, *Int. J. Heat Mass Transfer* **34,** 1149–1161 (1991).
5. N. Kasagi, Y. Tomita and A. Kuroda, Direct numerical simulation of the passive scalar field in a turbulent channel flow, *J. Heat Transfer* **114,** 598–606 (1992).
6. Y. G. Lai and R. M. C. So, Near-wall modeling of turbulent heat fluxes, *Int. J. Heat Mass Transfer* **33,** 1429–1440 (1990).
7. Y. Nagano and C. Kim, A two-equation model for heat transport in wall turbulent shear flows, *J. Heat Transfer* **110,** 583–589 (1989).
8. Y. Nagano, M. Tagawa and T. Tsuji, An improved two-equation heat transfer model for wall turbulent shear flows, *ASME-JSME Thermal Engng Proceedings*, Vol. 3, pp. 233–240 (1991).
9. Y. G. Lai and R. M. C. So, On near-wall turbulent flow modeling, *J. Fluid Mech.* **221,** 641–673 (1990).
10. R. M. C. So, Y. G. Lai, H. S. Zhang and B. C. Hwang, Second-order near-wall turbulence closures: a review, *AIAA J.* **29,** 1819–1835 (1991).
11. J. Kim, P. Moin and R. D. Moser, Turbulence statistics in fully developed channel flow at low Reynolds number, *J. Fluid Mech.* **177,** 133–186 (1987).
12. N. M. Mansour, J. Kim and P. Moin, Reynolds-stress and dissipation-rate budgets in a turbulent channel flow, *J. Fluid Mech.* **192,** 15–44 (1988).
13. R. M. C. So, H. S. Zhang and C. G. Speziale, Near-wall modeling of the dissipation-rate equation, *AIAA J.* **29,** 2069–2076 (1991).
14. R. M. C. So and T. P. Sommer, A near-wall eddy conductivity model for fluids with different Prandtl numbers, *J. Heat Transfer* **116,** 844–854 (1994).
15. A. F. Polyakov, Wall effect on temperature fluctuations in the viscous sublayer, *Teplofizika Vysokikh Temperatur* **12,** 328–337 (1974).
16. N. Kasagi, A. Kuroda and M. Hirata, Numerical investigation of near-wall turbulent heat transfer taking into account the unsteady heat conduction in the solid wall, *J. Heat Transfer* **111,** 385–392 (1989).
17. T. P. Sommer, R. M. C. So and H. S. Zhang, Heat transfer modeling and the assumption of zero wall temperature fluctuations, *J. Heat Transfer* **116,** 855–863 (1994).
18. T. Cebeci and P. Bradshaw, *Physical and Computational Aspects of Convective Heat Transfer*. Springer, New York (1984).
19. R. M. C. So, S. P. Yuan and T. P. Sommer, A hierarchy of near-wall closures for turbulent heat transfer, *Trends Heat Mass Momentum Transfer* **2,** 203–221 (1992).
20. M. M. Gibson and B. E. Launder, On the calculation of horizontal turbulent free shear flows under gravitational influence, *J. Heat Transfer* **98,** 81–97 (1976).
21. B. E. Launder, Heat and mass transport. In *Topics in Physics*, Vol. 12, *Turbulence* (Edited by Bradshaw), pp. 231–287. Springer, New York (1978).
22. S. Tavoularis and S. Corrsin, Effects of shear on the turbulent diffusivity tensor, *Int. J. Heat Mass Transfer* **28,** 265–276 (1985).
23. M. M. Rogers, N. N. Mansour and W. C. Reynolds, An algebraic model for the turbulent flux of a passive scalar, *J. Fluid Mech.* **203,** 77–101 (1989).
24. S. B. Pope, A more general effective viscosity hypothesis, *J. Fluid Mech.* **72,** 331–340 (1975).
25. T. B. Gatski and C. G. Speziale, On explicit algebraic stress models for complex turbulent flows, *J. Fluid Mech.* **254,** 59–78 (1993).
26. A. Yoshizawa, Statistical modelling of passive-scalar diffusion in turbulent shear flows, *J. Fluid Mech.* **195,** 541–555 (1988).
27. G. K. Batchelor, Diffusion in a field of homogeneous turbulence, *Austral. J. Sci. Res.* **A2,** 437–450 (1949).
28. T. P. Sommer and R. M. C. So, On the modeling of homogeneous turbulence in a stably stratified flow, *Phys. Fluids*, to appear (1995).
29. N. Kasagi and Y. Ohtsubo, Direct numerical simulation of low Prandtl number thermal field in a turbulent channel flow, *Turbulent Shear Flows* **8,** 97–119 (1992).
30. H. S. Zhang, R. M. C. So, C, G. Speziale and T. B. Gatski, A near-wall second-order closure for compressible turbulent flows. In *Near-Wall Turbulent Flows* (Edited by R. M. C. So *et al.*), pp. 209–218. Elsevier, Amsterdam, The Netherlands (1993).
31. R. M. C. So, H. Aksoy, T. P. Sommer and S. P. Yuan, Development of a near-wall Reynolds-stress closure based on the SSG model for the pressure strain, NASA Contractor Report 4618 (1994).
32. K. Bremhorst and K. J. Bullock, Spectral measurements of temperature and longitudinal velocity fluctuations in fully developed pipe flow, *Int. J. Heat Mass Transfer* **13,** 1313–1329 (1970).
33. M. Hishida, Y. Nagano and M. Tagawa, Transport processes of heat and momentum in the wall region of turbulent pipe flow, *Proceedings of the 8th International Heat Transfer Conference*, Vol. 3, pp. 925–930 (1986).
34. R. E. Johnk and T. J. Hanratty, Temperature profiles for turbulent flow of air in a pipe—I. The fully developed heat transfer region, *Chem. Engng Sci.* **17,** 867–879 (1962).
35. R. E. Johnk and T. J. Hanratty, Temperature profiles for turbulent flow of air in a pipe—II. The thermal entrance region, *Chem. Engng Sci.* **17,** 881–892 (1962).
36. A. F. Polyakov and S. A. Shindin, Development of turbulent heat transfer over the length of vertical tubes in the presence of mixed air convection, *Int. J. Heat Mass Transfer* **31,** 987–992 (1988).
37. B. S. Petukhov, A. F. Polyakov and Y. V. Tsypulev, Peculiarities of non-isothermal turbulent flow in horizontal plane channels at low Reynolds numbers and under significant buoyancy forces, *Turbulent Shear Flows* **2,** 158–167 (1980).
38. C. G. Speziale, S. Sarkar and T. B. Gatski, Modeling the pressure–strain correlation of turbulence: an invariant dynamical systems approach, *J. Fluid Mech.* **227,** 245–272 (1991).